Bull. Mater. Sci. (2018) 41:75
https://doi.org/10.1007/s12034-018-1593-3

Recent advances in titanium dioxide/graphene photocatalyst materials as potentials of energy generation

EPHRAIM M KIARII[1], KRISHNA K GOVENDER[2], PATRICK G NDUNGU[1] and PENNY P GOVENDER[1,*]

[1]Department of Applied Chemistry, University of Johannesburg, P.O. Box 17011, Doornfontein Campus, Johannesburg 2028, South Africa

[2]Council for Scientific and Industrial Research, Meraka Institute, Centre for High Performance Computing, Cape Town 7700, South Africa

*Author for correspondence (pennyg@uj.ac.za)

MS received 29 August 2017; accepted 18 April 2018

Abstract. The properties of titanium dioxide (TiO_2)/graphene/graphene oxides (GO) are examined in this study. These views summarize the recent theoretical and experimental novel approaches in the catalytic activity of TiO_2/graphene interface. Imperative results at a level of detail, suitable for upcoming experimental and theoretical researchers involved an overview of the enthralling characteristics of TiO_2 and graphene composites were presented. Aspects like crystal lattice, electronic band structure and phonon dispersion, among others that were used to describe the properties of a TiO_2 interface with pristine graphene and graphene dioxide among other composites are discussed. In particular, this review covers reactivity, binding energies, geometric structures as well as the photocatalytic activity of anatase TiO_2 surfaces with graphene and graphene oxide with hybrid nanocomposites. These views also explore the understanding of the TiO_2 interactions with graphene and possible applications. Finally, highlights on the challenges and proposed strategies in developing advanced photocatalytic semiconductor-based composites for water-splitting applications are provided.

Keywords. Titania; graphene; composites; *ab initio*; photocatalytic activity; semiconductor.

1. Introduction

The demand for clean water and energy has risen because of increased population and advancement in technology. Challenges of using non-renewable sources of energy are eminent; depletion of fossil fuels from source, disposal of nuclear wastes and evolution of greenhouse gases are some of them. Solar energy is a renewable source, its capture and conversion into electricity have become a great challenge to scientists and technologists [1]. Great scientific interest is being made in its storage as reduced fuels [2], oxygen from water [3–5] and chemical fuels [6–8]. Making solar hydrogen from water has become an area of intense research [9–15], giving rise to inexhaustible renewable fuel in the absence of pollutants and greenhouse gases. Harvesting energy from sunlight using photocatalytic or photoelectrocatalytic water-splitting and reduction of CO_2 with H_2O is considered as a viable means to save energy and the environment. Being a benchmark photocatalyst, TiO_2 is by far one of the most widely studied semiconductors [16–24].

Although significant research was done on TiO_2-based photocatalysts [25–32], the majority of research still lies in the development of environmental catalysis for the degradation of pollutants, such as dye and organic wastes. During recent decades, research on photocatalytic water-splitting and CO_2 reduction started to draw more attention. It should be noted that there are numerous publications reporting 'achievement' of H_2 production via water splitting using various kinds of sacrificial reagents, such as methanol, amine and amide among others [25,32–42]. However, it is worth noting that H_2 production reactions are not likely to be considered as a genuine 'water-splitting' reaction. This is because the photocatalytic water-splitting is the simultaneous split of water to yield O_2 and H_2 in the stoichiometric ratio of 1:2 under sunlight. Thus, the electrons used for the half reactions of proton reduction must be originally provided by the water oxidation half reaction. Simply, the O_2 evolution from water oxidation is inevitable for a genuine water-splitting reaction. The reactions with no observation of oxygen evolution are not true water splitting and therefore, they can only be referred as 'H_2 production reaction', 'H_2 evolution reaction', or 'half reaction of water-splitting'.

However, the working principle behind a good photocatalyst material lies on the synergistic effect of the materials involved in the system i.e., titania in this review (figure 1). Irradiance occurs in the UV region, electrons in the valence band (VB) are excited and move into the conduction band (CB) leaving holes in the VB [43]. However, the band structure, including the bandgap and the positions of VB and CB, is one of the important properties of a semiconductor because it

Published online: 19 May 2018

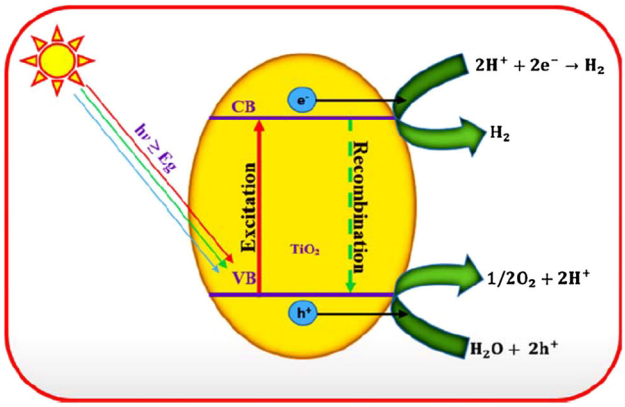

Figure 1. The synergistic effect of photocatalytic titania [47].

determines the light absorption property, as well as the redox capability of semiconductor and its application [44].

$$TiO_2 + hv \rightarrow e^- (TiO_2) + (TiO_2)\,. \tag{1}$$

In the TiO_2 lattice, the charge carriers may be captured as O^- and Ti^{3+} defect sites [45]. In some cases, the charge carriers may recombine to dissipate energy and eventually move to the catalyst surface to drive the redox reactions with the adsorbate (equation (2)) [46,47].

$$\text{Electrons } \left(e^-\right) + \text{holes } \left(h^+\right) \rightarrow \text{energy} \tag{2}$$

The reaction of positive holes (h^+) with H_2O on the catalyst surface may yield oxygen as illustrated in equation (3).

$$H_2O + 2h^+ \rightarrow \frac{1}{2}O_2 + 2H^+ \tag{3}$$

with the generated electrons on the CB may further be involved in the reduction reaction to yielding hydrogen (equation (4)).

$$2H^+ + 2e^- \rightarrow H_2. \tag{4}$$

The band alignments of TiO_2 anatase satisfy the criteria for the spontaneous splitting of water with its valence band maximum (VBM) and conduction band minimum (CBM) far lower than the water oxidation level (H_2O/O_2) and slightly higher than the H_2 generation level (H^+/H_2), respectively. The photogenerated holes (7.4 eV *vs*. vacuum) in TiO_2, which is lower than the highest occupied molecular orbitals of most organic pollutants, makes it easy for TiO_2 to oxidize organic pollutants in water [48]. Nonetheless, the wide energy gap of TiO_2 anatase (3.2 eV) restricts its application only to the UV region ($k < 380$ nm) [49]. Furthermore, the overall low quantum efficiency owing to the rapid recombination of photogenerated charge carriers is another drawback. Solar energy consists of 4–5% of UV light as opposed to 45% of visible light. Thus, prolonging its optical absorption spectrum into a longer wavelength region may have a significant impact on its practical applications. To improve the visible light response of TiO_2 anatase, several modifications, such as p-conjugated structure compositing [50], doping [51–54], coupling with other semiconductors [55–57] and dye sensitization are adopted.

Furthermore, H_2 production reactions using sacrificial reagents are thermodynamically favourable [58–61]. In such reactions, H_2 is produced with no net solar energy conversion into the form of chemical energy, although it may not be referred to as solar fuel. The efficiencies of water splitting and CO_2 photoreduction on TiO_2 are still rather low and far from the requirement of industrial applications. This is due to the intrinsic limitations of TiO_2 [62–64], which can absorb only UV light i.e., in the solar spectrum. However, with emerging new ideas, new methods, new theories and new materials, there could be some progress in solving the key scientific problems of solar energy conversion on TiO_2-based photocatalysts. From recent advances on the photocatalytic production of H_2 and photoreduction of CO_2 with H_2O on TiO_2-based photocatalysts, a better understanding of the complicated photocatalytic processes of H_2 production, water splitting and the CO_2 reduction could be obtained. It is important to consider improving the efficiency of all these processes simultaneously in an integrated system. The future research directions for TiO_2 can be identified through several routes: first, development of novel strategies or methods to enable TiO_2 absorbance in the longer wavelength of sunlight, band gap engineering by the co-doping of TiO_2 with metal cations and anions, surface sensitization of TiO_2 with visible light absorbing dyes, molecular complexes, quantum dots, etc. Although these strategies are promising for improving the absorption in the visible region i.e., red shift, they still suffer from some fatal problems. For example, doping of TiO_2 usually also creates charge recombination defect sites [65,66], and the dyes or molecular complexes are usually unstable [67], especially in the highly oxidizing environment of overall water splitting and CO_2 reduction with H_2O. Novel strategies for enhancing the light absorption of TiO_2 are highly desired. Second is the development of novel methods for improved separation of photo-induced holes and electron in TiO_2-based photocatalysts. Efficient charge separation is the vital step for improving the entire efficiency of solar energy conversion. It seems assembly of multicomponent integrated photocatalytic systems by a combination of these different strategies would be an ideal approach for achieving efficient charge separation. To assemble such a system, tailored design and manipulating of the interfaces/junctions between the redox matching functional components with proper built-in electric field/potential difference are extremely important. In terms of the semiconductor approach, co-catalysts and junctions are actually involved in improving the photocatalytic activity.

This review is aimed at understanding the theoretical and experimental aspects of the interaction of TiO_2 with

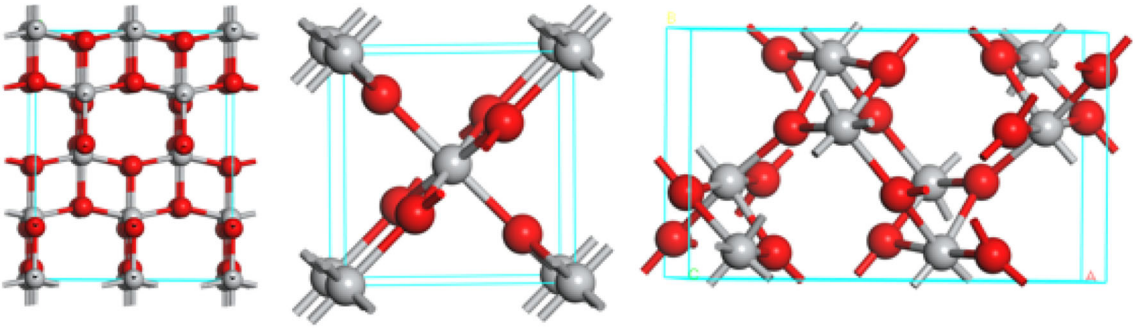

Figure 2. Structural models of anatase, rutile, brookite crystals, respectively. Red and grey spheres represent O and Ti, respectively.

Table 1. Structural parameters of body centred tetragonal TiO_2 (anatase) [147].

	Lattice parameter (Å)					Primitive cell		
Structure	A	B	C	Space group	Atom	Atomic position		
TiO_2	3.7842	3.7842	9.5146	141	Ti	0.0000	0.0000	0.0000
					Ti	0.7500	0.2500	0.5000
					O	0.2081	0.2081	0.0000
					O	0.9581	0.4581	0.5000
					O	0.7919	0.7919	0.0000
					O	0.5419	0.0419	0.5000

A, B and C represent lattice constants in three dimensions, Ti and O represent titanium and oxygen atoms, respectively.

graphene or graphene oxide (GO) and hybrids by investigating the interface properties of TiO_2 composites. Focus is based on recent research articles in TiO_2–graphene composites, especially on clean phase and bulk surfaces of anatase, the activities of anatase surfaces, pristine graphene (PG) and graphene oxide, TiO_2–graphene nanocomposites, photocatalytic efficiency and TiO_2 nanosheets/graphene hybrids. Great emphasis was placed on the fundamental mechanisms of the emerging strategies involved in the enhancement of TiO_2 photocatalytic activity as composites using graphene as well as graphene oxide. Since the interface chemistry is most important in the efficiencies of photocatalytic activity, understanding their applications in the visible light region is paramount.

2. TiO_2

TiO_2 was used in pigmentation, gas sensing, degradation of pollutants, inactivation of bacteria, dye degradation, solar cells among others [68–72]. TiO_2 has experienced much research in the past decade owing to its qualities such as stability, well characterized and is inexpensive when compared to other valuable semiconductors. The crystalline form of titania was found to influence its physical–chemical properties. TiO_2 exists mainly in three polymorphs, namely rutile, brookite and anatase as illustrated in figure 2.

Crystal structures of the three polymorphs are defined by the TiO_6 octahedral structure with different orientations of the octahedral in the patterns of the octahedral chains built. Both anatase and rutile have a tetragonal bulk unit cell, which is made up of titanium ions (Ti^{4+}) at the centre of an octahedron of six oxygen (O^{2-}) ions, and the two polymorphs mainly differ by distortion inside the octahedron, whereas in brookite, the oxygen atoms differ in two positions with different bond lengths amidst the titanium and oxygen atoms. Lattice parameters of anatase are provided in table 1.

The relatively large band gap of TiO_2 and its an impediment to its photo-activity to the wavelength region of ultraviolet emission ($\lambda < 387$ nm) [73]. To overcome this, two approaches were effectively employed: (a) band gap engineering and (b) surface sensitization. Semiconductor sensitization with metal synthesized quantum dots such as gold through bi-functional linker mercapto-acetic acid [74] has gained high attention owing to the exceptional optical and electronic properties of metallic clusters [75–80]. Metallic nanoparticles have exciting properties, which arise with the resultant interaction of CB electrons and the magnetic field [81–85].

In addition, there is a high recombination rate of electrons and hole pairs of TiO_2 which may probably be due to the generated charge carriers with less energy to reach the surface. Some are retained in the defective sites of the bulk caused by deformation during doping, while others recombine at the edges and generate heat or photons. The

Table 2. PBE surface energies (J m^{-2}) of low-index computed for relaxed (E^{rel}) and unrelaxed (E^{unr}) anatase TiO_2 surfaces [81].

Surface	(101)	(100)	(001)	(110)
E^{unr}	1.28	1.59	1.12	2.17
E^{rel}	0.49	0.58	0.98	1.15

electronic structure and phonon density of state play a major role in charge transfer and recombination inter-band distances and the large energy gap results in reduced photoactivity. To mitigate this drawback, the use of graphene nanosheets was employed. Graphene materials exhibit high crystallinity and mobility of charge carriers as well as good mechanical strength [86]. Therefore, these carbon-based materials enable charge transfer and inhibit the charge recombination process when combined with TiO_2-based photocatalysts.

Reactivity of TiO_2 chemical is governed by choice of the surface subjected to the reaction. The surface energies of the (100), (101), (110) and (001) surfaces of anatase are found to differ.

2.1 *Phases and surfaces of TiO_2*

Rutile is the stable phase of TiO_2, while both anatase and brookite are metastable; the latter is difficult to synthesize and so is seldom studied [87]. Lazzeri and co-workers [84] studied the low index and bulk phase surfaces of the rutile and anatase polymorphs of TiO_2. Their results on structural and elastic properties were in outstanding agreement with previous experimental data [80]. Diebold [78] investigated the surface energies of (100), (101), (110) and (001) surfaces of anatase TiO_2. The results showed that (101) was the most stable relaxed surface (table 2).

In addition, the marginal surface in unrelaxed TiO_2 was attributed to the instability of the (001) surface. Barmparis *et al* [79,80] showed that the construction produced a reduced bipyramid (figure 3). Diebold *et al* [80] described the atomic arrangement of (101) and (001) surfaces. They found that the (001) surface contains six-fold corresponding cations (Ti-6c) and two-fold-coordinated O anions (O-2c) (figure 3a). However, the (101) surface showed six-fold-coordinated Ti ions (Ti-6c) and three-fold-coordinated O ions (O-3c) (figure 3b). They concluded that the surface reactivity is not influenced by these ions.

Reactivity of anatase surfaces was studied by Vittadini and co-workers [82] using water adsorption to understand the reaction at the TiO_2 surface. Their results showed that the (001) surface produced a much resilient interface ($E_{ads} \sim 1.4$–1.6 eV), while the (101) surface adsorption produced inadequately bound ($E_{ads} \sim 0.7$ eV) molecular types. In addition, the (101) surface assembly was not disturbed by the adsorbent, while the (001) surface underwent a major rearrangement with the water dissociation, distracting one of the bonds of the bridging oxygen (figure 4). Lazzeri *et al* [84] showed that the reactivity of the linking oxygen in (001) surface agreed well with the experimental observations. In addition, their Wulff construction showed that the (101) and (001) surfaces were the only two exposed to vacuum.

2.2 *Computational studies on TiO_2*

Theoretically, several studies were carried out to investigate TiO_2 clusters [88–90]. Wu and Wang [91] found a theoretical TiO_2 band gap of 1.90 eV less than the experimental band gap of 3.0–3.2 eV. They attributed the difference to the inability of density functional theory (DFT) to estimate band gaps close to experimental data [92] as well as the size of cluster and bulk matter. Wu and Wang [91] also found a band gap of 2 eV for a $(TiO_2)_n$ (n = 1–4) cluster. They ascribed this low theoretical value to the lower coordination numbers. Albaret and co-workers [88] observed the same low band gap for $(TiO_2)_n$ (n = 1–3) clusters. They concluded that the low band gap was because of the excitonic quantum-size effects. Similar results were also reported by Auvinen *et al* [90].

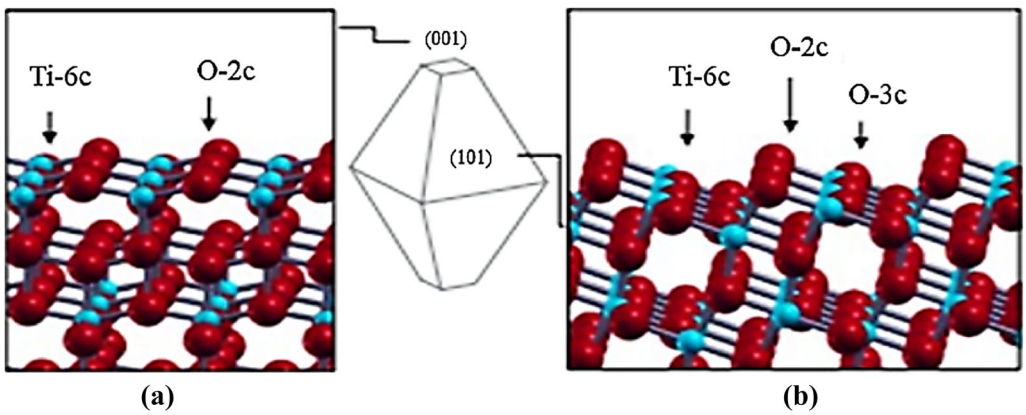

Figure 3. Equilibrium shapes for the atomic structures of minority (**a**) (001) and (**b**) (101) of the anatase TiO_2 crystal. Red and blue spheres represent O and Ti ions, respectively [81].

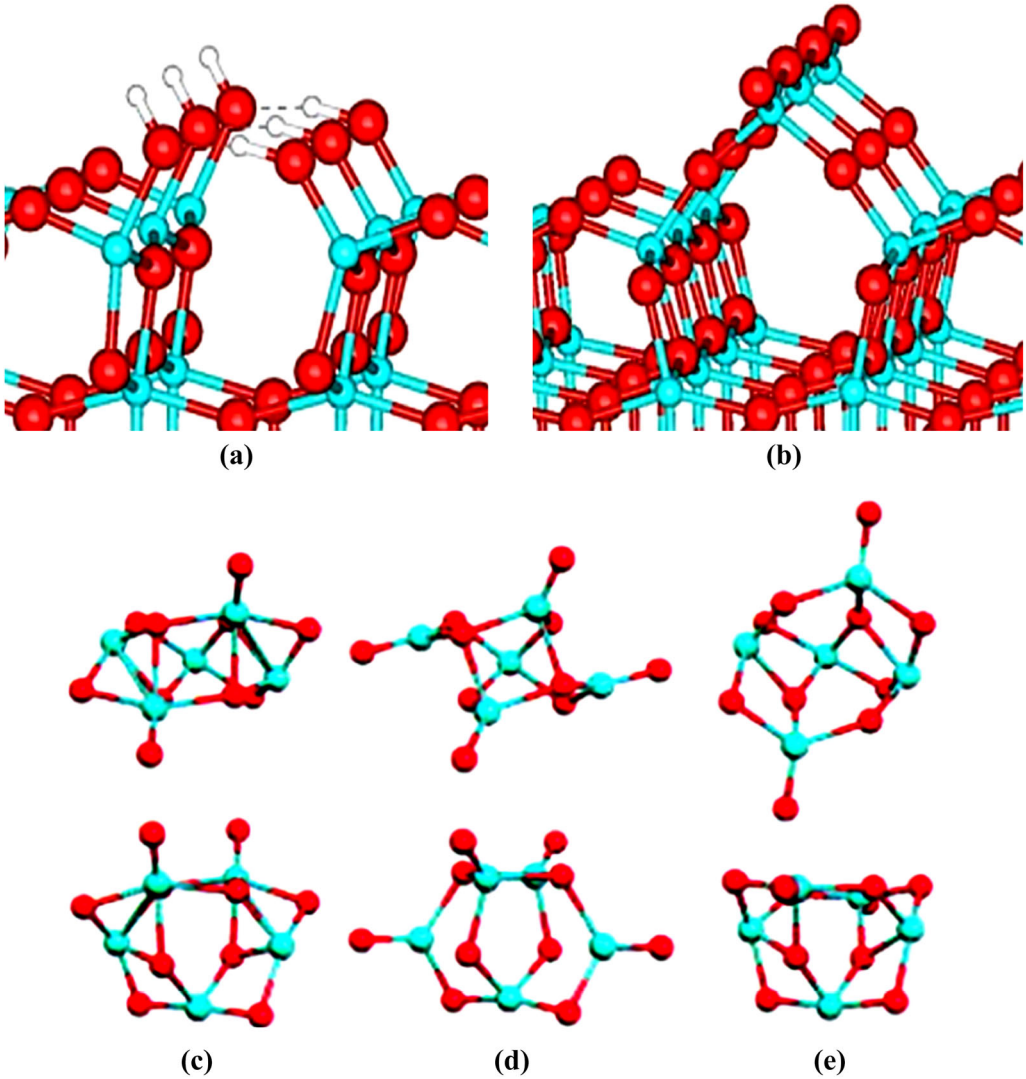

Figure 4. Atomic structures covered by (**a**) (001) surface with 0.5 ml of water [82], and (**b**) reconstructed clean (001) surface with added molecule [84] with hydrogen, oxygen and titanium represented by white, red and blue dots, respectively. Top and side views of the three $(TiO_2)_5$ structures: (**c**) (PW/VSZ), (**d**) (B3LYP/VDZ), (**e**) (B3LYP/LANL2DZ) [93], where oxygen and titanium are represented in red and blue dots, respectively.

Lundqvist *et al* [93] used frozen and relaxed cluster geometries (figure 4) and found different band gaps applying various basis sets and functionals as illustrated in table 3. Cluster A was found after relaxing the geometry with the same connectivity through the PW/SZ method. Using the same starting structure, cluster B was obtained with the B3LYP/VDZ basis set, while cluster C was obtained from the re-optimization of cluster A using B3LYP/LANL2DZ basis set. These three clusters were considered using several basis sets and functionals either in relaxing the geometries or after re-optimization with the specified method.

Further studies show improvement on the theoretical bandgap of TiO_2 moving it closer to the experimental value. Such an approach is the use of hybrid functionals on the DFT and additional parameters like Hubbard parameter [44,53]. It is worth noting that the increase in basis set leads to overestimation of the band gap. Other studies on TiO_2 were conducted on its ability to degrade dyes in the chromophore–TiO_2 interface [94,95], generate energy in the TiO_2-B lithium battery anode material [96], catechol and water interaction studied using *ab initio* molecular orbital theory and DFT [97]. Four anthracene-based sensitizers were designed and fabricated to illustrate the binding modes of anchoring groups with nanocrystalline TiO_2 (101) surface and on the effectiveness of dye-sensitized solar cells [98].

To improve the charge transfer rates and storage, the TiO_2 semiconductors–graphene composites were used due to their excellent thermal conductivity and high crystallinity in their

Table 3. Electronic structure for $(TiO_2)_5$ clusters, A, B and C band gaps in eV [93].

Type of cluster	Functional	Basis set	Band gap		
			a	b	c
Frozen geometries	Pw	SZ	1.57	2.73	1.72
		SZ-NC	1.61	2.72	1.76
		DZ	2.35	2.58	2.44
		DZ-NC	2.37	2.67	2.52
		TZP	2.34	2.66	2.46
		TZP-NC	2.36	1.77	2.55
	B3LYP	6-31G	4.07	4.65	4.23
		6-31G (d,p)	4.14	4.80	4.37
		6-31+G (d,p)	4.12	4.76	4.36
		6-311+G (2df,p)	—	4.83	4.44
	LDA	6-31+G (d,p)	2.41	2.74	2.58
	PW91	6-31+G (d,p)	2.49	2.81	2.60
	BLYP	6-31+G (d,p)	2.39	2.78	2.54
	HF	6-31+G (d,p)	11.17	12.86	11.54
Relaxed geometries	B3LYP	6-31G (d,p)	—	4.64	—
		6-31+G (d,p)	—	4.61	—
		6-311+G (2df,p)	—	4.64	—

structure. They can be easily formed into wires, thin sheets, nanoribbons and nanotubes.

3. Graphene

3.1 *PG*

In the last decade, studies on graphene have intensified owing to its unique properties. Graphene is a carbon-based compound, the ability of carbon to bond with other elements results in its application in several devices. Graphene has a hexagonal lattice structure, which is sp^2-hybridized [99]. It can easily be separated from graphite by peeling off its layers. To obtain the different conformations i.e., armchair, a chiral and zigzag tubes, graphene sheet can be cut and rolled into different directions forming carbon nanotubes. These can result in semiconductive and metallic structures. Graphene chemistry was extensively researched during the last two decades for its exceptional thermal, mechanical and electrical properties. These properties make it an interesting material in several applications ranging from batteries, sensors, nanoelectronics, hydrogen storage and supercapacitors [75,85,100–103].

Perfect graphene has a zero band gap [104–107]. Much research was done on how to tune the band gap in graphene-based semiconductor materials [108]. The band gap tuning can be achieved in PG via nanopatterning [109,110], application of gate voltage [111–114], or chemical functionalization [115–117]. The large-scale manufacture of PG sheets remains challenging and so is a cost-effective production method. Vapour phase graphene synthesis is a bottom-up approach used in syntheses, such as epitaxial growth and chemical vapour deposition. They yield large-size, thickness-controllable and high-quality grapheme [115,118,119], which could be compatible with device industry fabrication methods. Nevertheless, these substrate-based methods are limited in cost and scale, and cannot meet the requirement of macroscopic quantities of graphene for applications, such as coatings, advanced composites, energy storage and conductive ink. However, liquid-phase exfoliation (LPE) [120,121] of graphite into graphene has recently proved as a scalable method. Through LPE method, the mass production of reduced graphene oxide (rGO) and graphene nanoplatelets was achieved. Nevertheless, a major challenge remains in realizing high-quality and large-quantity fabrications of large-size thin few-layer graphenes (FLG).

3.2 *GO*

GO is an oxidized product of graphite, which has different compositions with several oxidation levels based on the synthesis conditions and processes of interest. GO can have hydroxyl, epoxy and carboxyl groups. The hydroxyl–epoxy functionalized graphene and GO are found in the same material. rGO has less functional groups than GO because the reduction process removes them. The solubility of GO in ethanol, water and among other liquids can be utilized as precursors for establishing large-scale graphene. GO being a functionalized product of the infusible and insoluble pure graphene sheets, is flexible and can be modified as a semiconductor, an insulator, or semi-metal having potential

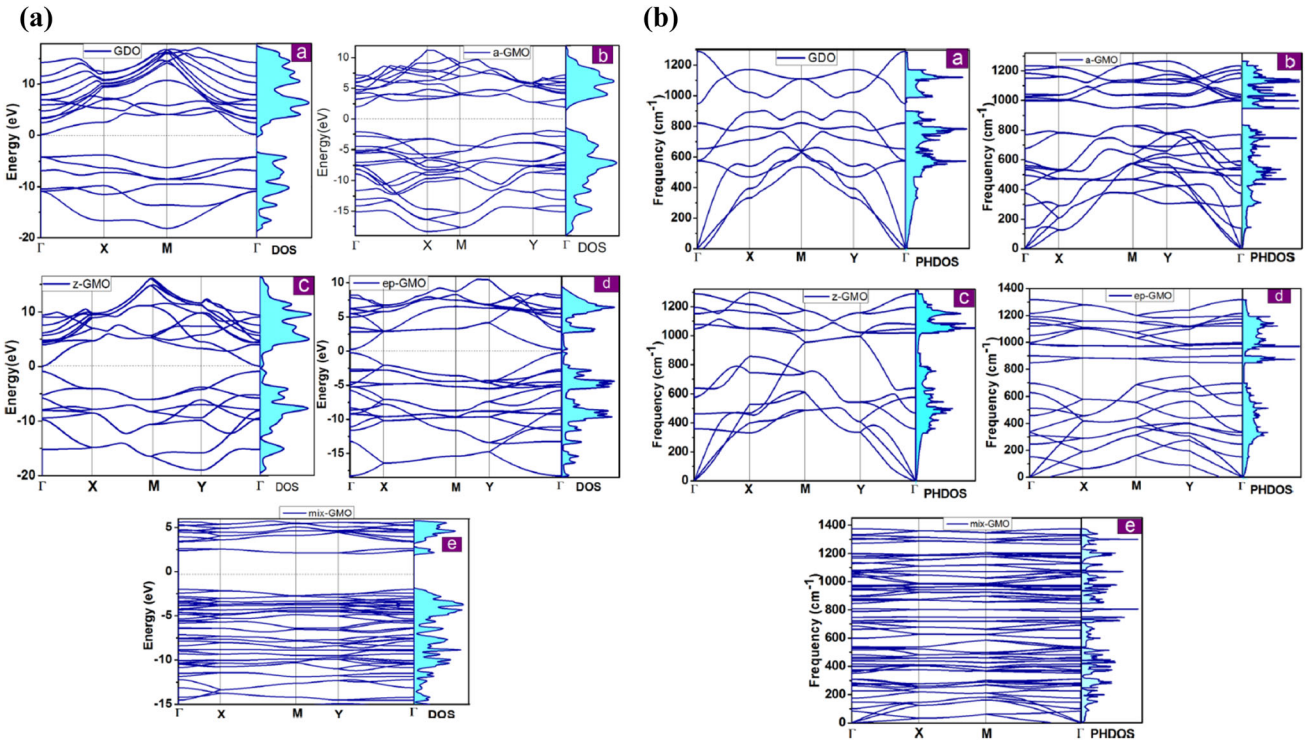

Figure 5. (**a**) Phonon dispersion curves of (a) GDO, (b) a-GMO, (c) z-GMO, (d) ep-GMO and (e) mix-GMO along with the corresponding phonon density of states. (**b**) Electronic band structures of (a) GDO, (b) a-GMO, (b) z-GMO, (c) ep-GMO and (e) mix-GMO in the Brillouin zone along with electronic density of states [126].

for wiring with bio- and organic-molecules. Zhang *et al* [122] proposed a model during his theoretical studies of graphene oxide, but the model could not predict the atomic structure of GO when compared to highly accurate synchrotron-based experimentally determined X-ray absorption near edge measurements [123]. The epoxy pair arrangement is used for a low energy structural model for stoichiometric graphene oxides in theoretical calculations [124,125]. Recently, Dabhi *et al* [126] proposed either type configuration as the ground state of the stoichiometric graphene oxide. They observed that the zigzag-graphene monoxide (z-GMO) and armchair-graphene monoxide (a-GMO) have lower energies and are more stable than the epoxy-graphene monoxide (ep-GMO) and mixed-graphene monoxide (mix-GMO) reported earlier by Xiang *et al* [124]. In addition, the molecular dynamics study shows that graphene dioxide (GDO), which was not yet synthesized, is unstable at high temperatures in contrast to the z-GMO, which is stable up to 2000 K [122].

The *ab initio* approach has used to interpret the electronic, structural, phonon and elastic properties of different models of graphene oxide, such as GDO, a-GMO and mix-GMO structures. The calculated elastic stiffness lattice parameters [126], phonon frequencies (figure 5a) and band structures (figure 5b) were found to agree with the theoretical data obtained by Kumar *et al* [127].

The zero temperature phonon dispersion curves confirmed the dynamical and mechanical stabilities of GO in GDO, a-GMO and mix-GMO structures. However, the electronic band structure in figure 5b and the total energy calculation supports the semiconducting nature for all of the above-considered structures and reveals the electronic stability of the z-GMO and ep-GMO structures of the graphene monoxides. The band structures revealed that the considered GO structures have band gap from 0.8 to 4 eV subject to the assemblies of graphene oxide. The wide range of energy gap available with GO suggests their potential applications in nanodevices.

The electronic properties of GO rely on chemical structure [128,129]. The epoxidefunctional group together with a hydroxyl group on graphene can cause a significant local distortion. Theoretical studies were conducted on the GO [53,130,131] and of significant interest is the dissemination of these functional groups on graphene. Recently, atomic force microscope (AFM) measurement revealed that the oxidized graphene sheets have a thickness equal to integer multiples of $h \approx 6.7$ Å [132], signifying that hydroxyl and epoxide groups are most likely to be bonded on both sides of the graphene sheet. This significantly affects the bonding characteristics of carbon changing from planar sp^2 to partial sp^3 hybridization. Considering an arrangement of epoxy functional group in fully oxidized graphene sheet and the effect of epoxy arrangement on electronic properties on graphene sheets with a molecular C:O ratio of 1:1 [125], structural parameters [126] (Å) of a-GMO, GDO, z-GMO, mix-GMO and ep-GMO are built using Cambridge Serial Total Energy Package in Material studio 2016, as shown in figure 6.

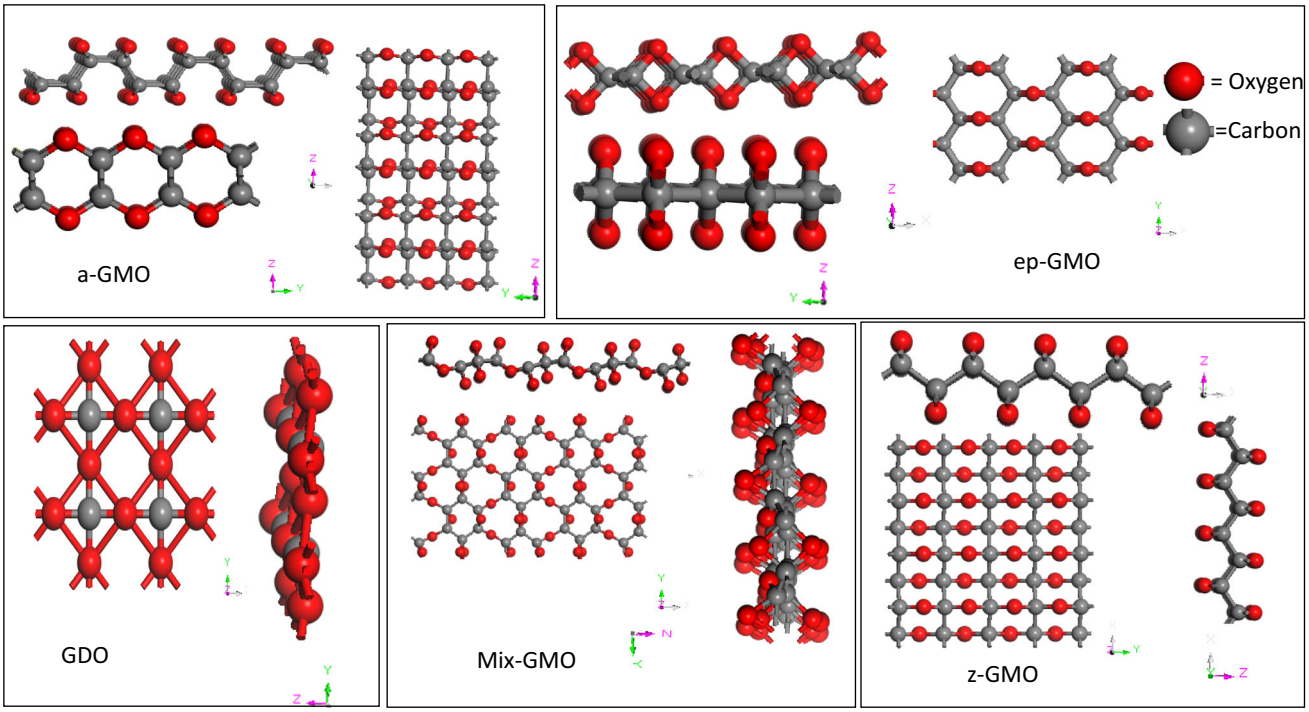

Figure 6. Atomic structures of a-GMO, ep-GMO, GDO, mix-GMO and z-GMO, along the xy, yz, xz planes. Calculated from lattice parameters [126].

3.3 *Carbon nanotubes (CNTs)*

Large scale production of CNTs is completed through chemical vapour deposition (CVD) techniques, proficient in meeting the anticipated characteristics for combined applications, bulk production, specificity, high purity, acceptable quality and low cost. CVD has commonly used the method to graft CNTs into fibre surface [133,134].

TiO_2 nanoparticles when used with multiwalled carbon nanotubes (MWCNTs) produce an improved photocatalytic activity [134]. Some fascinating results with earlier work [134–136] using titanium on MWCNTs reported excellent physisorbed systems with improved photoactivity. The reason for the improvement was attributed to the long lifetime of the photoinduced charge carriers that finally yield large quantities of radicals, the CNTs gave added sorption properties, and the composites had greater visible light sorption properties [137,138]. However, TiO_2/CNTs were used to make heterojunctions in the materials and thus improve photocatalytic efficiency [134].

4. TiO_2/graphene nanocomposites

Rojas *et al* [139] studied the theoretical behaviour of a titanium/graphene and water on the surface. The calculated DFT results of graphene/Ti-modified nanocomposites in interaction with various adsorbates to compare their adsorption process. The graphene nanocomposites from the theoretical study reveal similar results compared to previous studies on H adsorption [139]. The result revealed the responsive nature of oxygen molecule toward titanium adsorbed on graphene. Chemisorption of graphene with a binding energy of −8 eV and oxidation reaction occurred spontaneously when titanium adatom to TiO_2. The adornment of the graphene sheet using Ti permits storage up to four hydrogen molecules per adatom with an average binding energy of –0.42 eV per molecule. However, some of the oxygen molecules in 2H/Ti/graphene nanocomposites are expected to oxidize the titanium adatom to TiO_2, thereby altering the adsorption site to a top rotated position. Subsequently, the TiO_2 binds to the graphene sheet by a strong chemical bond. The energy barrier of H_2 molecule formed from the adsorbed atomic hydrogen was reduced to 0.74 eV compared to 1.74 eV when Ti incorporates on the graphene sheet. The TiO_2 can coordinate up to four hydrogen molecules, which remain physisorbed with a weak bonding interaction. Nevertheless, only the first two hydrogen molecules provide an interesting binding energy to the surface.

Long *et al* [140] studied graphene/TiO_2 composites and found an outstanding potential for photovoltaic uses, which provided an efficient photoinduced charge separation at the interface. The mechanisms and electronic structure of the photoinduced interfacial energy and charge transfer as well as energy relaxation were investigated in a hybrid graphene/TiO_2 system using the atomistic and real-time nonadiabatic molecular dynamics with time-dependent DFT. The calculations imitate the experimentally observed time-resolved energy

relaxation and electron transfer processes, which account for the mechanisms of the transfer of energy and charge through the nanocomposite [140]. The electron transfer from the graphene sheet to TiO_2 occurred on the ultrafast time scale owing to the strong acceptor–donor connection, favouring photoexcitation. The succeeding evolution followed by quick nonadiabatic changes down the various delocalized states, resultant in concurrent, electron-vibrational and energy transfer as well as energy relaxation. The noncovalent interaction was found between graphene and monolayer rutile TiO_2 (110) surface. Although the oxygen atoms, which can form additional chemical bonds did not disturb the π-electron system of graphene at all temperatures [140]. Due to the thermal excitation of out-of-plane motions of graphene, a 0.6 Å at room temperature was found when graphene transfers from the TiO_2 surface. These modes influence the π-electron system, thereby changing oscillations of the graphene electronic energy levels. High-frequency carbon bond stretching and bending modes add to the photoexcited (PE) electron dynamics to provide strong electron–vibrational coupling. The electronic acceptor–donor interaction is significant to a much wider range of atomic motions compared to the electronic energy. The former oscillates randomly on time scale longer than 10 fs, while the latter displays coherent oscillations prolonging into the picosecond range. The energy and electron transfer in graphene/TiO_2 nanocomposites can proceed in both the directions based on the energy of the excited electron. Once the electron relaxes to the bottom of the TiO_2 CB, it can transfer back onto graphene, since graphene has energy levels within the TiO_2 band gap. The back-transfer process can compete with the electron delocalization into the bulk TiO_2, which is driven by entropy. The detailed atomistic insights into the photoinduced electron-vibrational dynamics at the graphene/TiO_2 interface offer significant applications in nanoscience, photovoltaics, electrolysis and catalysis [140].

Yang *et al*'s [141] study on the electronic properties and chemical structure of two-dimensional titania/graphene, carbon-supported/titania and titania/graphdiyne composites calculated using DFT. Calculation displays that titania (001)/graphdiyne composites have superior oxidation properties and charge separation, extended lifetimes of photoexcited charge carriers in all the composites with different facets of titania. The experimental results showed titania (001)/graphdiyne composites as a favourable photocatalyst material with enhanced photocatalytic degradation towards methylene blue. The rate constant of titania (001)/graphdiyne composite is 0.15 and 0.12 times compared to the bulk TiO_2 and titania (001)/graphene composite, respectively. Through first-principles of DFT study, the electronic properties and chemical structure of TiO_2/graphene and TiO_2/graphdiyne composites with different TiO_2 facets are calculated. The TiO_2 (001)/graphdiyne composite displays excellent oxidation ability, electronic structure and charge separation than that of pure TiO_2 (001) and TiO_2 (001)/graphene composite, which makes it an ideal photocatalyst material. Theoretical prediction is that the TiO_2 (001)/graphdiyne composite reveals enhanced photocatalytic activity compared with TiO_2 (001)/graphene composites and other 2D carbon-based TiO_2 composites. Therefore, we anticipate that graphdiyne may be an excellent co-catalyst among the 2D carbon materials in the field of photovoltaics and photocatalysis.

Long [142] studied the electronic structure of titania (110) surface incorporated with both metallic and semiconducting carbon nanotube through DFT study. The results showed improved absorbance in the visible solar region as compared to ultraviolet region owing to effective interfacial charge separation. Thus, the semiconducting titania/carbon nanotube can be applied in photovoltaic material. Moreover, the strong interaction between a metallic titania and carbon nanotube enhances the charge transfer to induce a built-in potential [142]. Immobilizing the metallic carbon nanotube with a small platinum cluster increases the built-in potential to improve the separation of charge carriers. These observations signify that the carbon nanotube/titania interface can be an ideal potential photovoltaic material.

The performed first-principles calculations using DFT explored charge transfer and electronic properties at the interface formed between rutile (110) surface and CNTs in the perspective of photovoltaic cells and a visible light photocatalyst. Immobilization of either metallic carbon nanotube or a semiconducting into the titania lattice induces band gap reduction. The band gap reduction signifies the slight improvement of photocatalytic performance under simulated ultraviolet light irradiation. However, an electron can be transferred from the first or second von Hove singularity of the carbon nanotube between the VB and CB under visible-light irradiation. Then, the photogenerated electron transferred into the CB of titania can significantly reduce the transition energy to enhance the photocatalytic activity. Due to efficient charge separation across the interface of semiconducting carbon nanotube/titania with reference to the metallic carbon nanotube/titania, the former is better than the latter as photocatalysts and photovoltaic materials. A substantial charge transfer occurs from the metallic carbon nanotube to the titania and subsequently, a small built-in potential could be unfavourable for exciton dissociation. Observations reported by Long [142] reveal that the carbon nanotube/titania heterojunction composites are efficient to improve the photocurrent via metal-cluster-decorated CNTs.

Liu *et al* [143] studied graphene/TiO_2 nanocomposites anode materials for lithium ion batteries and display much higher lithium storage capacity beyond their theoretical capacity, but the mechanisms are still poorly understood [143]. Through first-principles total energy calculations, an all-inclusive understanding of microscale of the discharge procedure of graphene/TiO_2 containing surface, bulk and interfacial lithium storage is studied. The results showed that interfacial oxygen atoms play a vital role in the interfacial lithium storage. The additional capacity originating from the surface and interfacial lithium storage through an electrostatic capacitive mechanism significantly contribute to the electrode capacity. This reveals that the nanocomposites used in energy

Table 4. Binding energy (E_b), equilibrium graphene–cluster distance (d) and charge transfer (ΔQ) of TiO_2 cluster anchoring on different graphene sheets [73].

Substrate	E_b (eV)	(Å)	$\Delta Q_{cluster}$ (C)
P-G	−1.08	2.64	0.33
V-G	−2.43	2.20	0.10
O-G	−3.21	1.91	−0.11

storage material, electrode and capacitor behaviours can be optimized to design high-performance electrode materials with the balance of storage rate and capacity. Adsorption at the graphene/TiO_2 (001) interface is around interfacial oxygen atoms, and with Li adsorption at the interface, the reduction process of GO benefits electrical conductivity. During the surface and interface storage processes, surface and interfacial O atoms serve as hosts for Li^+ and bond with Li atoms via valence-like and ionic bonds, respectively, while graphene serves as an electron acceptor, resulting in a charge separation. Surface and interface storage processes contribute to additional Li storage capacity beyond the theoretical capacity via an interfacial pseudo-capacity-like storage mechanism. The discharge process of graphene-modified TiO_2 can be divided into the surface, bulk and interface storages, with surface and bulk storages contributing to the monotonous potential drop and potential plateau and interface storage contributing to the slope potential drop in the discharge curve. The research results present a comprehensive understanding of the discharge process of graphene/metal oxide, which indicate the possibility of designing electrode materials with high capacity and fast charging/discharging rates through an interfacial storage mechanism in graphene/metal oxide nanocomposite electrodes.

Geng *et al*'s [73] study on the photocatalytic efficiency of TiO_2–graphene nanocomposites shown that TiO_2 does not absorb in the visible region of the light spectrum. However, when combined with grapheme, there is the possibility of improving the absorption in the visible region. Further, they studied the photocatalytic properties of TiO_2 composites with defect graphene (VG), PG and GO using DFT calculations. They observed electron redistribution and polarization for all the composites. In comparison to VG and PG, GO interface with the TiO_2 anatase cluster displayed a larger binding energy and stronger electron cloud overlap (table 4).

In addition, they concluded that the photocatalytic performance of the various nanocomposites resulted in the electrons excitation from the O 2p state on the VBM to the C 2p state on the CBM. They attributed the improved photocatalytic performance to the band gap reduction and the reduced recombination rate of electrons and holes by graphene. Further studies were conducted by Masuda *et al* [144] using graphene hybrids.

Other studies on possible opportunities or potential applications of graphene/TiO_2 composites (table 5) are referenced.

5. Hybrids

Zhang *et al* [145] fabricated a hybrid ternary TiO_2/graphene/CdS on GO via an *in situ* approach. The ternary graphene/TiO_2/CdS hybrid exhibited an improved photocatalytic performance compared to the matrix binary graphene/CdS. The enhanced photocatalytic activityis ascribed to the larger surface area, excellent interfacial charge transfer rate and longer lifetime of photogenerated charge carriers. Thus, the graphene-based composites improve the photocatalytic processes. Xiang *et al* [146] explored the generation of H_2 via photocatalytic water splitting process. TiO_2 nanocrystals incorporated onto hybrid MoS_2/graphene, exhibited a high photocatalyst performance for H_2 evolution. This reveals an inexpensive nonnoble photocatalyst for energy conversion with efficient H_2 evolution. Moreover, titania-based composite photocatalysts with a layered MoS_2/graphene co-catalyst showed an operational photocatalyst for H_2 production via a two-step hydrothermal method. The as-prepared composite exhibited an enhanced photocatalytic H_2 generation with a rate of 165.3 μmol h^{-1} for the 0.5% MG hybrid catalyst. The enhanced interfacial charge transfer suppresses charge recombination and provides a greater number of active adsorption sites as well as photocatalytic reaction centres due to the synergetic effect between the MoS_2 and graphene sheets.

Masuda *et al* [144] successfully studied the interfacial interaction between graphene and anatase TiO_2 (001) surface. In the study, they modelled, optimized and explored the various properties, which included the electronic properties of graphene/TiO_2 hybrids using DFT implemented in VASP code with the generalized gradient approximation of Perdew–Burke–Ernzerhof pseudo-potentials and the projector augmented waves approach to treat the electron–ion interactions. The results revealed a physical adsorption system being less electronically attached and did not increase the photoresponsivity in the visible region. However, for the bonding between graphene and TiO_2 nanosheets, a Ti–O–C bridge made the two components highly electronically combined. For the GO/TiO_2 adsorption, which involves a chemical reaction between the surface system was exemplified by a higher photoresponsivity in the visible light. It was thus, ascribed to the formation of a new VBM that lay in the pristine energy gap of TiO_2 nanosheets, because of GO and TiO_2 hybrid. Their further study on chemisorption and physisorption in water observed that the band structures of the studied models at the CBM of graphene and TiO_2 nanosheets were nearly at the same energy level close to GO (figure 7) and this agrees with the experimental results [125], where (d = dry, w = wet) in d_1, d_2, w_1 and w_2.

Using Bader charge partitioning method, the interfacial charge transfer was evaluated. The results reveal that in the two-physisorbed systems, the charge was strongly localized compared to the chemisorbed systems. A workfunction (Φ) was used to understand the origin of charge transfer. The calculated workfunction difference ($\Delta\Phi$) was large in the

Table 5. Graphene/TiO_2 composite applications.

Opportunities and applications of graphene/TiO_2 composites	Ref.
Graphene over titanium dioxide applied in photocatalysts	[148–152]
Dye-sensitized solar cell and photoanodes	[153–155]
Photoactivity of titanium dioxide/graphene nanotubes for removal of acetaminophen	[156]
Photoconductor for inkjet printable ionic solution	[157]
A graphene/titanium dioxide nanocomposite for application in a solid rocket propellant	[158]
Disinfection of water	[159–163]
High-performance supercapacitors	[164–166]
TiO_2/graphene photoelectron chemical biosensing at a low potential	[167–172]

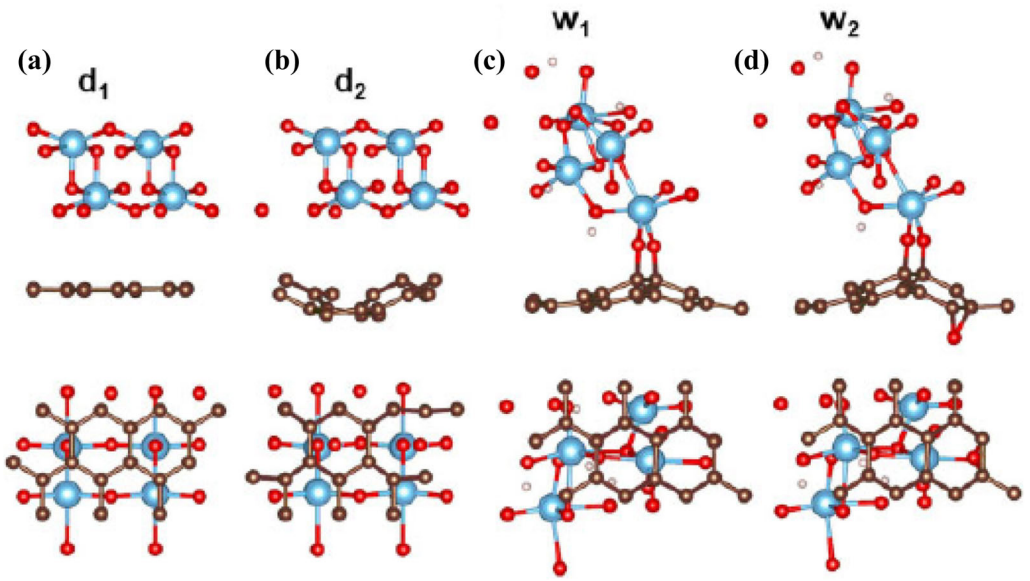

Figure 7. Side and top views of graphene–TiO_2 bilayer nanocomposite models with physisorbed (**a**) d_1 and (**b**) d_2 hybrid models and (**c**) w_1 and (**d**) w_2 models [144].

Table 6. Charge transfer (ΔQ) from graphene to TiO_2 nanosheets in the ground state, work function (Φ) and work function difference ($\Delta\Phi$) [144].

	d_1	d_2	w_1	w_2
ΔQ	0.019	0.015	0.083	0.040
Graphene (Φ)	3.886	4.224	6.701	6.586
TiO_2(Φ)	6.741	7.096	6.905	7.071
$\Delta\Phi$	2.885	2.872	0.204	0.485

physisorbed system; this was in favour of finding a chemical bond that has the delocalized charge. Oxygen in GO layer added the electronegativity and caused a reduction in charge flow in the w_2 compared to w_1 models inducing electron accumulation in TiO_2 nanosheets (n-type) and a hole in graphene (p-type) (table 6).

6. Conclusions and outlook

Recent *ab initio* and experimental studies involving TiO_2 and graphene composites were reviewed. Focus was on the interface properties and their influence on the properties of the composites. Titania clean surfaces and bulk phase study have considered. Based on this review, the following conclusions can be made:

1. The (101) surface is the most stable. Thus, the (101) phase can be used to determine the chemistry of anatase TiO_2, but both the (001) surface and defects on (101) plays a leading role in reactivity. Adsorption on (101) produced weak bonds stronger than the (001).
2. The results on electronic, structural, phonon and elastic properties revealed band gap enlargement in GO over PG and this suggests potential applications in nanodevices.

3. On photocatalytic properties of the titania composites, the interface structures, binding energy, electron total charge density and projected density of state shows improved photocatalytic performance in the integrated composites promising applications in photocatalysis.
4. Hybrid composites of bilayer anatase (001) show that physisorbed systems are less electronically coupled and do not extend the photocatalytic activity into the visible region compared to chemisorbed systems as a result of the formation of a new VBM state that lies in the pristine band gap of TiO_2 nanosheets.

A better understanding of the mechanisms for the photocatalytic reaction processes, including light harvesting, carrier migration and transport, with the elementary reactions involving atomic or molecular level, is necessary for the improvement of TiO_2 composites for various solar energy conversion efficiencies. Only with a comprehensive understanding of all these processes as guidance, efficient TiO_2-based photocatalytic systems may be developed. Combining time- and space-resolved spectroscopic techniques with computational studies, more in-depth knowledge on charge separation in TiO_2-based photocatalysts could be obtained. Due to the intrinsic limitations, TiO_2 may not be the promising photocatalyst for solar fuels generation by means of the photocatalytic splitting of water and CO_2 photoreduction. It is thus not expected that a great breakthrough in solar fuels production might occur on TiO_2-based photocatalysts, but as shown in this review, TiO_2 might be an ideal model of semiconductor-based photocatalysts.

Acknowledgements

We would like to acknowledge the financial contributions from the Faculty of Science: University of Johannesburg-South Africa: Centre for Nanomaterials Science Research, Department of Applied Chemistry and the National Research Foundation (TTK14052167682). EMK acknowledges the financial support from National Research Foundation (NFF) and Global Excellence and Stature (GES) from the University of Johannesburg. We are also grateful to the Centre for High Performance Computing (CHPC) for computational resources provided.

References

[1] Zamfirescu C and Dincer I 2014 *Solar Energy* **107** 700
[2] Agbossou K, Kolhe M, Hamelin J and Bose T K 2004 *IEEE Trans. Energy Convers.* **19** 633
[3] Kanan M W and Nocera D G 2008 *Science* **321** 1072
[4] Evans A, Strezov V and Evans T J 2012 *Renew. Sust. Energ. Rev.* **16** 4141
[5] Gorlin Y and Jaramillo T F 2010 *J. Am. Chem. Soc.* **132** 13612
[6] Kodama T 2003 *Prog. Energy Combust. Sci.* **29** 567
[7] Joshi U A, Palasyuk A, Arney D and Maggard P A 2010 *J. Phys. Chem. Lett.* **1** 2719
[8] Asi M A, Zhu L, He C, Sharma V K, Shu D, Li S *et al* 2013 *Catal. Today* **216** 268
[9] Steinfeld A 2002 *Int. J. Hydrogen Energ.* **27** 611
[10] Tamaura Y, Steinfeld A, Kuhn P and Ehrensberger K 1995 *Energy* **20** 325
[11] Bard A J and Fox M A 1995 *Acc. Chem. Res.* **28** 141
[12] Bolton J R 1996 *Solar Energy* **57** 37
[13] Bak T, Nowotny J, Rekas M and Sorrell C 2002 *Int. J. Hydrogen Energ.* **27** 991
[14] van de Krol R, Liang Y and Schoonman J 2008 *J. Mater. Chem.* **18** 2311
[15] Charvin P, Abanades S, Flamant G and Lemort F 2007 *Energy* **32** 1124
[16] Ding Z, Lu G Q and Greenfield P F 2000 *J. Phys. Chem. B* **104** 4815
[17] Yu J C, Yu J, Ho W, Jiang Z and Zhang L 2002 *Chem. Mater.* **14** 3808
[18] Kawahara T, Konishi Y, Tada H, Tohge N, Nishii J and Ito S 2002 *Angew. Chem.* **114** 2935
[19] Li N, Liu G, Zhen C, Li F, Zhang L and Cheng H M 2011 *Adv. Funct. Mater.* **21** 1717
[20] Kong M, Li Y, Chen X, Tian T, Fang P, Zheng F *et al* 2011 *J. Am. Chem. Soc.* **133** 16414
[21] Kumar S G and Devi L G 2011 *J. Phys. Chem. A* **115** 13211
[22] Habisreutinger S N, Schmidt-Mende L and Stolarczyk J K 2013 *Angew. Chem. Int. Ed.* **52** 7372
[23] Lin Z, Orlov A, Lambert R M and Payne M C 2005 *J. Phys. Chem. B* **109** 20948
[24] Akhavan O and Ghaderi E 2009 *J. Phys. Chem. C* **113** 20214
[25] Kozlova E A, Korobkina T P, Vorontsov A V and Parmon V N 2009 *Gen. Appl. Catal. A* **367** 130
[26] Zamfirescu C, Dincer I, Naterer G F and Banica R 2013 *Chem. Eng. Sci.* **97** 235
[27] Huang L, Wang X, Yang J, Liu G, Han J and Li C 2013 *J. Phys. Chem. C* **117** 11584
[28] Sasaki Y, Iwase A, Kato H and Kudo A 2008 *J. Catal.* **259** 133
[29] Bae S W, Ji S M, Hong S J, Jang J W and Lee J S 2009 *Int. J. Hydrogen Energ.* **34** 3243
[30] Fu X, Yang H, He K, Zhang Y and Wu J 2013 *Mater. Res. Bull.* **48** 487
[31] Kozlova E A, Korobkina T P and Vorontsov A V 2009 *Int. J. Hydrogen Energ.* **34** 138
[32] Bamwenda G R and Arakawa H 2001 *Sol. Energy Mater. Sol. Cells* **70** 1
[33] Galinska A and Walendziewski J 2005 *Energ. Fuel.* **19** 1143
[34] Kudo A and Miseki Y 2009 *Chem. Soc. Rev.* **8** 253
[35] Ni M, Leung M K, Leung D Y and Sumathy K 2007 *Renew. Sust. Energy Rev.* **11** 401
[36] Kudo A 2006 *Int. J. Hydrogen Energ.* **31** 197
[37] Zou Z, Ye J, Sayama K and Arakawa H 2001 *Nature* **414** 625
[38] Ke D, Peng T, Ma L, Cai P and Jiang P 2008 *Appl. Catal. A* **350** 111
[39] Pappacena A, Boaro M, Šolcová O and Trovarelli A 2017 *J. Phys. Chem. C* **33** 17746
[40] Casallas C, Dincer I and Zamfirescu C 2016 *Int. J. Hydrogen Energ.* **41** 7969
[41] Jiang D, Sun Z, Jia H, Lu D and Du P 2016 *J. Mater. Chem. A* **4** 675

[42] Zhou X, Jin J, Zhu X, Huang J, Yu J, Wong W-Y *et al* 2016 *J. Mater. Chem. A* **4** 5282
[43] Oppong S O-B, Anku W W, Shukla S K, Agorku E S and Govender P P 2016 *J. Sol–Gel Sci. Technol.* **80** 38
[44] Kiarii E M, Govender K K, Ndungu P G and Govender P P 2017 *Chem. Phys. Lett.* **678** 167
[45] Tachikawa T, Fujitsuka M and Majima T 2007 *J. Phys. Chem. C* **111** 5259
[46] Cozzoli P, Comparelli R, Fanizza E, Curri M and Agostiano A 2003 *Mater. Sci. Eng. C* **23** 707
[47] Opoku F, Govender K K, van Sittert C G C E and Govender P P 2017 *Int. J. Quantum Chem.* **e25505**, https://doi.org/10.1002/qua.25505
[48] Xu P, Xu T, Lu J, Gao S, Hosmane N S, Huang B *et al* 2010 *Energ. Environ. Sci.* **3** 1128
[49] Yin W-J, Tang H, Wei S-H, Al-Jassim M M, Turner J and Yan Y 2010 *Phys. Rev. B* **82** 045106
[50] Li Q, Zong L, Xing Y, Wang X, Yu L and Yang J 2013 *Sci. Adv. Mater.* **5** 1316
[51] Dozzi M V and Selli E 2013 *J. Photochem. Photobiol. C: Photochem. Rev.* **14** 13
[52] Devi L G, Murthy B N and Kumar S G 2010 *Mater. Sci. Eng. B* **166** 1
[53] Kiarii E M, Govender K K, Ndungu P G and Govender P P 2017 *Computat. Condens. Matter*, https://doi.org/10.1016/j.cocom.2017.08.003
[54] Rauf M, Meetani M and Hisaindee S 2011 *Desalination* **276** 13
[55] Park H, Park Y, Kim W and Choi W 2013 *J. Photochem. Photobiol. C: Photochem. Rev.* **15** 1
[56] Kubacka A, Munoz-Batista M J, Ferrer M and Fernández-García M 2013 *Appl. Catal. B* **140** 680
[57] Kiarii E M, Govender K K, Ndungu P G and Govender P P 2017 *Chem. Phys. Lett.* **680** 69
[58] Hisatomi T, Kubota J and Domen K 2014 *Chem. Soc. Rev.* **43** 7520
[59] Leung D Y, Fu X, Wang C, Ni M, Leung M K, Wang X *et al* 2010 *ChemSusChem* **3** 681
[60] Huang B-S, Chang F-Y and Wey M-Y 2010 *Int. J. Hydrogen Energ.* **35** 7699
[61] Maeda K, Hashiguchi H, Masuda H, Abe R and Domen K 2008 *J. Phys. Chem. C* **112** 3447
[62] Noworyta K and Augustynski J 2004 *Electrochem. Solid State Lett.* **7** E31
[63] Zhu W, Qiu X, Iancu V, Chen X-Q, Pan H, Wang W *et al* 2009 *Phys. Rev. Lett.* **103** 226401
[64] Hendry E, Koeberg M, O'regan B and Bonn M 2006 *Nano Lett.* **6** 755
[65] Tao F F, Schneider W F and Kamat P V 2015 *John Wiley & Sons* **1** 191
[66] Coker V S, Green M, Corr S, Imai H and Haigh S 2012 *RSC Adv.* **1** 145
[67] Di Valentin C, Pacchioni G, Selloni A, Livraghi S and Giamello E 2005 *J. Phys. Chem. B* **109** 11414
[68] Gauthier S, Reisberg B, Zaudig M, Petersen R C, Ritchie K, Broich K *et al* 2006 *Lancet* **367** 1262
[69] Fernández-García M, Martínez-Arias A, Hanson J C and Rodriguez J A 2004 *Chem. Rev.* **104** 4063
[70] Linsebigler A L, Lu G and Yates J T 1995 *Chem. Rev.* **95** 735
[71] Maeda K, Teramura K, Lu D, Takata T, Saito N, Inoue Y *et al* 2006 *Nature* **440** 295
[72] Fujihira M, Satoh Y and Osa T 1981 *Nature* **293** 206
[73] Geng W, Liu H and Yao X 2013 *Phys. Chem. Chem. Phys.* **15** 6025
[74] Huang Q, Chen J, Zhao J, Pan J, Lei W and Zhang Z 2015 *Nanoscale Res. Lett.* **10** 1
[75] Berger C, Song Z, Li X, Wu X, Brown N, Naud C *et al* 2006 *Science* **312** 1191
[76] Car R and Parrinello M 1985 *Phys. Rev. Lett.* **55** 2471
[77] Lazzeri M, Vittadini A and Selloni A 2002 *Phys. Rev. B* **65** 119901
[78] Diebold U 2003 *Surf. Sci. Rep.* **48** 53
[79] Barmparis G D, Lodziana Z, Lopez N and Remediakis I N 2015 *Beilstein J. Nanotechnol.* **6** 361
[80] Diebold U, Ruzycki N, Herman G S and Selloni A 2003 *Catal. Today* **85** 93
[81] Lazzeri M, Vittadini A and Selloni A 2001 *Phys. Rev. B* **63** 155409
[82] Vittadini A, Selloni A, Rotzinger F P and Grätzel M 1998 *Phys. Rev. Lett.* **81** 2954
[83] Vittadini A, Casarin M and Selloni A 2007 *Theor. Chem. Acc.* **117** 663
[84] Lazzeri M and Selloni A 2001 *Phys. Rev. Lett.* **87** 266105
[85] Peumans P 2008 *Appl. Phys. Lett.* **92** 263302
[86] Berger C, Wu X, Brown N, Naud C, Li X, Song Z *et al* 2006 *Science* **312** 1191
[87] Beltran A, Gracia L and Andres J 2006 *J. Phys. Chem. B* **110** 23417
[88] Albaret T, Finocchi F and Noguera C 2000 *J. Chem. Phys.* **113** 2238
[89] Tsipis A and Tsipis C 1999 *Phys. Chem. Chem. Phys.* **1** 4453
[90] Auvinen S, Alatalo M, Haario H, Jalava J-P and Lamminmäki R-J 2011 *J. Phys. Chem. C* **115** 8484
[91] Wu H and Wang L S 1997 *J. Phys. Chem. C* **107** 8221
[92] Mori-Sánchez P, Cohen A J and Yang W 2008 *Phys. Rev. Lett.* **100** 146401
[93] Lundqvist M J, Nilsing M, Persson P and Lunell S 2006 *Int. J. Quantum Chem.* **106** 3214
[94] Duncan W R and Prezhdo O V 2007 *Annu. Rev. Phys. Chem.* **58** 143
[95] Nilsing M, Persson P, Lunell S and Ojamäe L 2007 *J. Phys. Chem. C* **111** 12116
[96] Arrouvel C, Parker S C and Islam M S 2009 *Chem. Mater.* **21** 4778
[97] Redfern P, Zapol P, Curtiss L, Rajh T and Thurnauer M 2003 *J. Phys. Chem. B* **107** 11419
[98] Srinivas K, Yesudas K, Bhanuprakash K, Rao V J and Giribabu L 2009 *J. Phys. Chem. C* **113** 20117
[99] Cooper D R, D'Anjou B, Ghattamaneni N, Harack B, Hilke M, Horth A *et al* 2012 *ISRN Condens. Matter Phys.* **2012** 1
[100] Zhang Y, Tan Y W, Stormer H L and Kim P 2005 *Nature* **438** 201
[101] Novoselov K S, Geim A K, Morozov S V, Jiang D, Zhang Y, Dubonos S V *et al* 2004 *Science* **306** 666
[102] Ritter K A and Lyding J W 2009 *Nat. Mater.* **8** 235
[103] Miao F, Wijeratne S, Zhang Y, Coskun U C, Bao W and Lau C N 2007 *Science* **317** 1530
[104] Xu Y, Kraft M and Xu R 2016 *Chem. Soc. Rev.* **45** 3039
[105] Tsai H-S, Hsiao C-H, Chen C-W, Ouyang H and Liang J-H 2016 *Nanoscale* **8** 9488
[106] Cao X, Shi J, Zhang M, Jiang X, Zhong H, Huang P *et al* 2016 *J. Phys. Chem. C* **38** 21202

[107] Auton G, Zhang J, Kumar R K, Wang H, Zhang X, Wang Q *et al* 2016 *Nat. Commun.* **7** 11670
[108] Gupta S K, Soni H R and Jha P K 2013 *AIP Adv.* **3** 032117
[109] Han M Y, Zyilmaz B, Zhang Y and Kim P 2007 *Phys. Rev. E* **98** 1
[110] Giovannetti G, Khomyakov P A, Brocks G, Kelly P J and Van Den Brink J 2007 *Phys. Rev. B* **76** 2
[111] Molitor F, Jacobsen A, Stampfer C, Güttinger J, Ihn T and Ensslin K 2009 *Phys. Rev. B* **79** 075426
[112] Ryzhii V and Ryzhii M 2009 *Phys. Rev. B* **79** 1
[113] Avetisyan A A, Partoens B and Peeters F M 2009 *Phys. Rev. B* **80** 195401
[114] Dragoman M, Neculoiu D, Deligeorgis G, Konstantinidis G, Dragoman D, Cismaru A *et al* 2010 *Appl. Phys. Lett.* **97** 093101
[115] Wu X, Sprinkle M, Li X, Ming F, Berger C and De Heer W A 2008 *Phys. Rev. Lett.* **101** 26801
[116] Jung I, Dikin D A, Piner R D and Ruoff R S 2008 *Nano Lett.* **8** 4283
[117] Elias D C, Nair R R, Mohiuddin T M, Morozov S V, Blake P, Halsall M P *et al* 2009 *Science* **323** 610
[118] Zhang Y, Zhang L and Zhou C 2013 *Acc. Chem. Res.* **46** 2329
[119] Wang L, Tian L-H, Wei G-D, Gao F-M, Zheng J-J and Yang W-Y 2011 *J. Inorg. Mater.* **26** 1009
[120] Randviir E P, Brownson D A and Banks C E 2014 *Mater. Today* **17** 426
[121] Coleman J N 2012 *Acc. Chem. Res.* **46** 14
[122] Zhang S, Zhou J, Wang Q and Jena P 2013 *J. Phys. Chem. C* **117** 1064
[123] Saxena S, Tyson T A and Negusse E 2010 *J. Phys. Chem. Lett.* **1** 3433
[124] Xiang H, Wei S-H and Gong X 2010 *Phys. Rev. B* **82** 1
[125] Mattson E C, Pu H, Cui S, Schofield M A, Rhim S, Lu G *et al* 2011 *ACS Nano* **5** 9710
[126] Dabhi S D, Gupta S D and Jha P K 2014 *J. Appl. Phys.* **115** 203517
[127] Kumar A, Li D and Bahadur D 2013 *Carbon* **57** 346
[128] Mermoux M, Chabre Y and Rousseau A 1991 *Carbon* **29** 469
[129] He H, Klinowski J, Forster M and Lerf A 1998 *Chem. Phys. Lett.* **287** 53
[130] Li J-L, Kudin K N, McAllister M J, Prud'homme R K, Aksay I A and Car R 2006 *Phys. Rev. Lett.* **96** 176101
[131] Boukhvalov D W and Katsnelson M I 2008 *J. Am. Chem. Soc.* **130** 10697
[132] Pandey D, Reifenberger R and Piner R 2008 *Surf. Sci.* **602** 1607
[133] Yang J, Zhang J, Zhu L, Chen S, Zhang Y, Tang Y*et al* 2006 *J. Hazard. Mater.* **137** 952
[134] Melchionna M, Marchesan S, Prato M and Fornasiero P 2015 *Catal. Sci. Technol.* **5** 3859
[135] Ramoraswi N O and Ndungu P G 2015 *Nanoscale Res. Lett.* **10** 1
[136] Hintsho N, Petrik L, Nechaev A, Titinchi S and Ndungu P 2014 *Appl. Catal. B* **273** 156
[137] Allen M J, Tung V C and Kaner R B 2009 *Chem. Rev.* **110** 132
[138] Elstner M, Porezag D, Jungnickel G, Elsner J, Haugk M, Frauenheim T *et al* 1998 *Phys. Rev. B* **58** 7260
[139] Rojas M I and Leiva E P M 2007 *Phys. Rev. B* **76** 155415
[140] Long R, English N J and Prezhdo O V 2012 *J. Am. Chem. Soc.* **134** 14238
[141] Yang N, Liu Y, Wen H, Tang Z, Zhao H, Li Y *et al* 2013 *ACS Nano* **7** 1504
[142] Long R 2013 *J. Phys. Chem. Lett.* **4** 1340
[143] Liu E, Wang J, Shi C, Zhao N, He C, Li J *et al* 2014 *ACS Appl. Mater. Interf.* **6** 18147
[144] Masuda Y, Giorgi G, Yamashita K and About I 2014 *Phys. Status Solidi B* **251** 1471
[145] Zhang N, Zhang Y, Pan X, Yang M-Q and Xu Y-J 2012 *J. Phys. Chem. C* **116** 18023
[146] Xiang Q, Yu J and Jaroniec M 2012 *J. Am. Chem. Soc.* **134** 6575
[147] Horn M, Schwerdtfeger C F and Meagher E P 1972 *Z. Kristallogr. Cryst. Mater.* **136** 273
[148] Wang J, Zhu H, Hurren C, Zhao J, Pakdel E, Li Z and Wang X 2015 *JECE* **3** 1437
[149] Sakthivel S and Kisch H 2003 *Angew. Chem. Int. Ed.* **42** 4908
[150] Williams G, Seger B and Kamat P V 2008 *ACS Nano* **2** 1487
[151] Liu S, Sun H, Liu S and Wang S 2013 *Chem. Eng. J.* **214** 298
[152] Liang Y, Wang H, Casalongue H S, Chen Z and Dai H 2010 *Nano Res.* **3** 701
[153] Sacco A, Porro S, Lamberti A, Gerosa M, Castellino M, Chiodoni A *et al* 2014 *Electrochim. Acta* **131** 154
[154] Yang N, Zhai J, Wang D, Chen Y and Jiang L 2010 *ACS Nano* **4** 887
[155] Wang J T-W, Ball J M, Barea E M, Abate A, Alexander-Webber J A, Huang J *et al* 2013 *Nano Lett.* **14** 724
[156] Tao H, Liang X, Zhang Q and Chang C-T 2015 *Appl. Surf. Sci.* **324** 258
[157] Manga K K, Wang S, Jaiswal M, Bao Q and Loh K P 2010 *Adv. Mater.* **22** 5265
[158] Dey A, Nangare V, More P V, Khan M A S, Khanna P K, Sikder A K *et al* 2015 *RSC Adv.* **5** 63777
[159] Fernández-Ibáñez P, Polo-López M, Malato S, Wadhwa S, Hamilton J, Dunlop P *et al* 2015 *Chem. Eng. J.* **261** 36
[160] Liu L, Bai H, Liu J and Sun D D 2013 *J. Hazard. Mater.* **61** 214
[161] Chang Y-N, Ou X-M, Zeng G-M, Gong J-L, Deng C-H, Jiang Y *et al* 2015 *Appl. Surf. Sci.* **343** 1
[162] Linley S, Liu Y, Ptacek C J, Blowes D W and Gu F X 2014 *ACS Appl. Mater. Interf.* **6** 4658
[163] Rahimi R, Zargari S, Yousefi A, Berijani M Y, Ghaffarinejad A and Morsali A 2015 *Appl. Surf. Sci.* **355** 1098
[164] Liu W-W, Yan X-B and Xue Q-J 2013 *J. Mater. Chem.* **1** 1413
[165] Xiang C, Li M, Zhi M, Manivannan A and Wu N 2012 *J. Mater. Chem.* **22** 19161
[166] Ramadoss A and Kim S J 2013 *Carbon* **63** 434
[167] Zeng X, Bao J, Han M, Tu W and Dai Z 2014 *Biosens. Bioelectron.* **54** 331
[168] Sun W, Guo Y, Ju X, Zhang Y, Wang X and Sun Z 2013 *Biosens. Bioelectron.* **42** 207
[169] Casero E, Alonso C, Petit-Domínguez M D, Vázquez L, Parra-Alfambra A M, Merino P *et al* 2014 *Microchim. Acta* **181** 79
[170] How G T S, Pandikumar A, Ming H N and Ngee L H 2014 *Sci. Rep.* **4** 5044
[171] Zhu S, Guo J, Dong J, Cui Z, Lu T, Zhu C *et al* 2013 *Ultrason. Sonochem.* **20** 872
[172] Jang H D, Kim S K, Chang H, Jo E H, Roh K M, Choi J-H *et al* 2015 *Aerosol Sci. Tech.* **49** 538